Crystal Structure of the All-Ferrous [4Fe-4S]^0 Form of the Nitrogenase Iron Protein from *Azotobacter vinelandii*[†,‡]

Pavel Strop,[§] Patricia M. Takahara,[||] Hsiu-Ju Chiu,[⊥] Hayley C. Angove,[#] Barbara K. Burgess,[#] and Douglas C. Rees*,[⊥]

Biochemistry Option, California Institute of Technology, Mail Code 147-75, Pasadena, California 91125, Division of Chemistry and Chemical Engineering, California Institute of Technology, Mail Code 147-75CH, Pasadena, California 91125, Department of Molecular Biology and Biochemistry, University of California, Irvine, California 92697-3900, and Howard Hughes Medical Institute and Division of Chemistry and Chemical Engineering, California Institute of Technology, Mail Code 147-75CH, Pasadena, California 91125

Received July 14, 2000; Revised Manuscript Received November 7, 2000

ABSTRACT: The structure of the nitrogenase iron protein from *Azotobacter vinelandii* in the all-ferrous [4Fe-4S]^0 form has been determined to 2.25 Å resolution by using the multiwavelength anomalous diffraction (MAD) phasing technique. The structure demonstrates that major conformational changes are not necessary either in the iron protein or in the cluster to accommodate cluster reduction to the [4Fe-4S]^0 oxidation state. A survey of [4Fe-4S] clusters coordinated by four cysteine ligands in proteins of known structure reveals that the [4Fe-4S] cluster of the iron protein has the largest accessible surface area, suggesting that solvent exposure may be relevant to the ability of the iron protein to exist in three oxidation states.

Biological nitrogen fixation is catalyzed by the nitrogenase system which consists of two metalloproteins: the iron protein (Fe protein) and the molybdenum iron protein (MoFe protein) (*1*−*5*). The Fe protein is an ∼64 kDa γ_2 dimer with a single [4Fe-4S] cluster bridging the two subunits, while the MoFe protein is an $\alpha_2\beta_2$ tetramer that contains two types of metalloclusters, the FeMo cofactor and the P cluster. The reduction of dinitrogen to ammonia by nitrogenase involves the reduction of the Fe protein by electron carriers such as ferredoxin and flavodoxin. The Fe protein subsequently transfers electrons to the MoFe protein in a MgATP-dependent process, followed by electron and proton transfer to the substrate. Each electron transfer step involves the association and dissociation of the Fe protein and MoFe protein complex. This cycle repeats until enough electrons are transferred to the substrate, which is most likely bound to the FeMo cofactor of the MoFe protein. In the current understanding of the nitrogenase mechanism, the [4Fe-4S] cluster of the Fe protein is believed to undergo a one-electron reduction cycle between the [4Fe-4S]$^+$ and [4Fe-4S]$^{2+}$ oxidation states.

In 1994, Watt et al. (*6*) reported that the [4Fe-4S]$^+$ state of the Fe protein can be further reduced to the all-ferrous [4Fe-4S]^0 state. The properties of an all-ferrous Fe protein produced by reduction with Ti(III) citrate have been extensively characterized by Burgess, Münck, and co-workers (*7*−*11*). The all-ferrous Fe protein has been shown to bind MgATP, undergo a MgATP-induced conformational change, form the productive complex with the MoFe protein, and transfer electrons to the MoFe protein, leaving the cluster of the Fe protein in the [4Fe-4S]$^{2+}$ oxidation state (*8*). It is unclear whether the transfer of electrons between proteins takes place one at a time or if both electrons can be transferred together. If the transfer starts at the [4Fe-4S]^0 state of the Fe protein, one ATP molecule can apparently be hydrolyzed for each electron that is transferred (*12*), rather than the two ATP molecules per electron observed from the [4Fe-4S]$^+$ state. Therefore, the ATP utilization process can potentially be twice as efficient through the all-ferrous state of the Fe protein. It has been suggested that both forms of the reduced Fe protein might be mechanistically competent (*12*).

Before the discovery of the all-ferrous Fe protein, protein-bound [4Fe-4S] clusters had been known to undergo either [4Fe-4S]$^{3+/2+}$ or [4Fe-4S]$^{2+/+}$ redox cycles, but not both (*13*). The [4Fe-4S] cluster of the Fe protein is the only known example of a protein-bound [4Fe-4S] cluster that can function in three oxidation states. Furthermore, no other [4Fe-4S] protein clusters or model compounds with thiolate ligands are known to exist in the all-ferrous [4Fe-4S]^0 oxidation state. Here we report a crystal structure of an all-ferrous state of

[†] This work was supported by the National Institute of Health (Grant GM43144 to B.K.B. and Grant GM45162 to D.C.R.), an NSF graduate fellowship (P.S.), and an NSF postdoctoral fellowship (P.M.T.). This work is based upon research conducted at the Stanford Synchrotron Radiation Laboratory (SSRL), which is funded by the Department of Energy (BES and BER) and the National Institutes of Health (NCRR and NIGMS). The Advanced Light Source is supported by the Director, Office of Energy Research, Office of Basic Energy Sciences, Materials Sciences Division, of the U.S. Department of Energy under Contract DE-AC03-76SF00098 at Lawrence Berkeley National Laboratory.

[‡] The coordinates for the structures have been deposited in the RCSB Protein Data Bank for release upon publication (entries 1G1M and 1G5P).

* To whom correspondence should be addressed. E-mail: dcrees@caltech.edu. Phone: (626) 395-8393. Fax: (626) 744-9524.

[§] Biochemistry Option, California Institute of Technology.

[||] Division of Chemistry and Chemical Engineering, California Institute of Technology.

[⊥] Howard Hughes Medical Institute and Division of Chemistry and Chemical Engineering, California Institute of Technology.

[#] University of California, Irvine.

10.1021/bi0016467 CCC: $20.00
Published on Web 12/21/2000

Table 1: Data Collection and Phasing Statistics[a]

	peak λ_1	inflection λ_2	remote λ_3	high-resolution
wavelength (Å)	1.737	1.741	1.378	1.08
resolution range (Å)	20−3.0	20−3.0	20−3.0	20−2.25
no. of unique observations	12779	12748	12222	28724
no. of total observations	66302	64197	55432	154673
completeness[b] (%)	97 (99.6)	97 (99.7)	94.4 (97.3)	93.2 (85.2)
R_{sym}[b,c]	6.4 (15.1)	5.7 (20.8)	7.1 (23.8)	5.4 (30.6)
$\langle I/\sigma \rangle$[b]	7.8 (4.0)	8.7 (3.1)	8.6 (2.8)	21.3 (3.8)
R_{cullis} (cen/acen/anom)[d]	0.72/0.59/0.85	0.64/0.50/0.86	−/−/0.91	
phasing power (cen/acen/anom)[e]	2.09/3.31/1.47	2.33/4.83/1.48	−/−/1.25	
figure of merit (cen/acen)	0.64/0.55			

[a] Phasing and heavy atom refinement statistics are calculated to 3.0 Å resolution, for centric and acentric reflections and anomalous difference data (cen, acen, and anom, respectively). [b] The numbers in parentheses indicate values for the highest-resolution bin (3.16−3.00 Å for λ_1, λ_2, and λ_3 and 2.33−2.25 Å for high-resolution). [c] $R_{sym} = \Sigma|I_{obs} - I_{avg}|/\Sigma I_{obs}$. [d] R_{cullis} = lack of closure error/average absolute isomorphous or anomalous difference. [e] Phasing power = rms heavy atom structure factor/lack of closure error.

the Fe protein at 2.25 Å resolution. Since there are no model compounds with thiolate ligands in this oxidation state, this work provides the first crystallographic view of an all-ferrous $[4Fe\text{-}4S]^0$ cluster.

METHODS

Protein Purification and Reduction to the [4Fe-4S]⁰ State. The *A. vinelandii* Fe protein (Av2)[1] was purified as described elsewhere (*14*). All experimental procedures were carried out in an anaerobic chamber with an oxygen level of <1 ppm. Ti(III) citrate and the Ti(III) citrate-reduced Fe protein were prepared as described previously (*7*, *8*, *15*). Ti(III) citrate was removed from the Fe protein on a Sephadex G-25 column, and the protein was concentrated in a Centricon-30 apparatus in an anaerobic centrifuge to a final concentration of 30 mg/mL in 20% glycerol, 450 mM NaCl, and 50 mM Tris (pH 8.0). It should be noted that the all-ferrous Av2 is pink whereas the $[4Fe\text{-}4S]^+$ state is brown. Exposure of the all-ferrous Av2 solution to oxygen immediately leads to oxidation of the cluster and to a dark brown solution.

Crystallization. Crystals were grown by the capillary microbatch method (*16*) with 20 μL of precipitant solution containing 26−29% PEG 4000, 700−900 mM NaCl, and 100 mM Tris (pH 8.0) and 10 μL of protein solution containing 30 mg/mL all-ferrous Av2 in 20% glycerol, 450 mM NaCl, and 50 mM Tris (pH 8.0). Pink crystals were obtained after 1 week and belonged to space group $P2_1$ (a = 57.0 Å, b = 93.3 Å, c = 62.8 Å, and β = 98.9°), which is similar to the crystal form obtained with molybdate described in the original structure determination (*16*). Molybdate could not be used in these crystallization studies, however, since the presence of this anion led to rapid oxidation of the all-ferrous form of Av2.

Data Collection and Structure Determination. Data were collected on frozen crystals, and the color of the crystals was monitored to ensure that data were collected on the all-ferrous state of the protein. At the end of the data collections, there appeared to be slight discoloration on the surfaces of the crystals; however, the crystals always remained predominantly pink. A high-resolution data set was collected at −160 °C on beamline 7-1 of the Stanford Synchrotron Research Laboratory (SSRL) (Table 1). The structure was initially determined by molecular replacement with AMORE (*17*) using the 2NIP structure as the search model. This model, however, could not be refined satisfactorily. At this point, experimental phases were determined to 3.0 Å resolution from a three-wavelength MAD data set collected at −160 °C on beamline 5.0.2 at the Advanced Light Source (ALS) (Table 1). The fluorescence spectrum measured around the Fe edge of a single crystal was used to select the inflection point (λ = 1.741 Å), the absorption edge (λ = 1.737 Å), and a high-energy remote wavelength (λ = 1.378 Å) for optimization of the anomalous signal. Data were processed with MOSFLM and scaled with the CCP4 program suite (*18*).

The initial position of the iron−sulfur cluster was taken from the molecular replacement solution and was consistent with the anomalous and dispersive difference Patterson maps. Positions and occupancies of the four cluster irons, as well as $\Delta f'$ and $\Delta f''$ values for three wavelengths, were refined by using the program SHARP (*19*). The initial phases were improved by solvent flattening and 2-fold noncrystallographic symmetry averaging (NCS) in DM (*20*). The model was initially refined to 3.0 Å resolution against SHARP-calculated Fourier coefficients based on the two-dimensional centroid of the probability distribution for the native complex structure factor (*19*). After the R_{free} dropped below 0.35, the model was refined against the higher-resolution (2.25 Å) native data set collected at SSRL, incorporating the lower-resolution test set reflections into the higher-resolution test set. Later in the refinement, individual *B*-factors were refined and the 2-fold NCS restraints were released. Alternate cycles of manual model building using the program O (*21*), positional and individual *B*-factor refinement with the programs CNS (*22*) and REFMAC (*18*), and addition of water molecules to the model reduced the *R*-factor and *R*-free to 0.238 and 0.289, respectively, where *R*-free is calculated for 5% of the reflections. The root-mean-square deviations (rmsds) of bond lengths and angles from ideal values are 0.012 Å and 1.66°, respectively, with 85.9% of the residues in the most allowed region and 14.1% in the additionally allowed region of the Ramachandran plot (*23*). The average *B*-factors are as follows: 53.5 Å^2 for the main chain, 55.5 Å^2 for side chains, 39.8 Å^2 for the cluster, and 59.3 Å^2 for the solvent. An average *B*-factor of 55.4 Å^2 is calculated for all protein atoms. The final model contains 4380 protein atoms, one [4Fe-4S]

[1] Abbreviations: 1NIP, 2.9 Å resolution structure of the *A. vinelandii* Fe protein; 1G5P, 2.2 Å resolution structure of the *A. vinelandii* Fe protein; 1CP2, 1.93 Å resolution structure of the *Clostridium pasteurianum* Fe protein; Av1, *A. vinelandii* MoFe protein; Av2, *A. vinelandii* Fe protein; Cp2, *C. pasteurianum* Fe protein; EXAFS, extended X-ray absorption fine structure spectroscopy; rmsd, root-mean-square deviation.

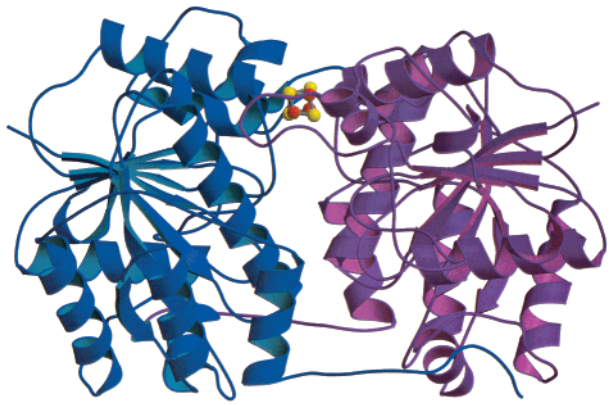

FIGURE 1: Ribbons diagram of the all-ferrous *A. vinelandii* Fe protein dimer. The [4Fe-4S] cluster at the dimer interface is represented by the ball-and-stick model. Subunits A and B are colored purple and blue, respectively. This figure was generated with Bobscript and Raster3D (*35*, *36*).

cluster, and 365 water molecules, for a total of 4753 atoms. No Ti(III) citrate or citrate was found bound to the protein.

During cluster refinement, the Fe−S bonds were restrained to 2.33 Å (bond energy of 700 kcal mol^{-1} $Å^{-2}$ in CNS), and the Fe−S−Fe and Fe−SG−CH_2 angles were weakly restrained (angle energy of 100 kcal mol^{-1} rad^{-2} in CNS) to 72° and 109°, respectively. No restraints were applied to the Fe−Fe or S−S distances during the refinement. For comparisons between the [4Fe-4S] clusters in different Fe protein structures, the 2NIP structure of the *A. vinelandii* Fe protein (*24*) was refined with the same cluster protocol as the all-ferrous Av2, resulting in the 1G5P model. In the 1G5P refinement, all atoms were held fixed except for the [4Fe-4S] cluster and the cysteine-containing loops (residues 96−98 and 131−133 in each monomer).

In the following discussion, the currently determined structures of Fe proteins will be designated as follows: the present 2.25 Å resolution all-ferrous Av2 structure (all-ferrous Av2), the initial 2.9 Å resolution Av2 structure in a monoclinic crystal form [PDB entry 1NIP (*16*)], the 2.2 Å resolution Av2 structure in an orthorhombic crystal form (PDB entry 1G5P) that represents a re-refinement of the 2NIP Fe protein structure (*24*) employing the same cluster restraints used for the all-ferrous structure, the 1.93 Å resolution *Clostridium pasteurianum* Cp2 [PDB entry 1CP2 (*24*)], and the Av1−Av2 complex stabilized with ADP·AlF_4^{-1} [PDB entry 1N2C (*25*)]. The oxidation states of the 1NIP, 1G5P, and 1CP2 structures have not been unambiguously established. While the initial crystallizations were conducted with the cluster in the dithionite-reduced $[4Fe\text{-}4S]^{+}$ state, it is possible that the protein oxidizes during the time required for crystallization (*26*), and could also become photoreduced during X-ray data collection (*27*). Consequently, the oxidation states of these Fe protein forms are not precisely defined, and will be collectively designated as "oxidized" without assignment of formal oxidation states.

RESULTS AND DISCUSSION

Protein Structure

Comparison to Other Fe Protein Structures. The all-ferrous Fe protein adopts the same overall conformation as the uncomplexed 1NIP and 1G5P Av2 structures (Figure 1).

Table 2: Fe−Fe and S−S Distances (in Å) in the [4Fe-4S] Cluster of Different Fe Protein Structures[a]

atom pair	all-ferrous Av2	1G5P	1CP2
Fe1−Fe2	2.67	2.71	2.72
Fe1−Fe3	2.79	2.64	2.62
Fe1−Fe4	2.57	2.67	2.60
Fe2−Fe3	2.69	2.70	2.64
Fe2−Fe4	2.54	2.56	2.54
Fe3−Fe4	2.66	2.71	2.67
S1−S2	3.72	3.66	3.64
S1−S3	3.82	3.72	3.72
S1−S4	3.86	3.80	3.76
S2−S3	3.64	3.73	3.69
S2−S4	3.74	3.68	3.74
S3−S4	3.68	3.65	3.67

[a] Fe1−Fe4 are coordinated by the Sγ of Cys B97, Cys A132, Cys A97, and Cys B132, respectively, while S1−S4 are the sulfurs opposite Fe3, Fe4, Fe2, and Fe1, respectively, in the [4Fe-4S] cubane.

In the structurally conserved β-sheet region, the rmsds in Cα positions relative to the all-ferrous Fe protein are 0.41 Å for 1NIP, 0.17 Å for 1G5P, 0.32 Å for 1CP2, and 0.4 Å for 1N2C in monomer A. With all Cα's, the corresponding rmsds are 0.65 Å for 1NIP, 1.10 Å for 1G5P, and 1.80 Å for 1N2C. The structure of the all-ferrous Av2 indicates small deviations from ideal NCS symmetry exist between the two monomers. The rmsd in the β-sheet region between the A and B subunits of the all-ferrous Av2 is 0.3 Å, while the rmsd for all Cα between the two subunits is 0.65 Å, a value similar to that of the 1G5P structure (0.62 Å). The regions with the largest conformational variation include the previously reported loop regions containing residues 37−47, 60−70, 90−101, 113−116, 128−136, and 171−175 (*24*). These loops adopt different conformations in the 1NIP and 1G5P structures. In the all-ferrous Av2, these loops exhibit conformations that are intermediate between the 1NIP and 1G5P conformations.

Structure and Environment of the $[4Fe\text{-}4S]^0$ Cluster

Cluster Geometry. This crystallographic analysis of the all-ferrous form of Av2 verifies that the cluster retains the general cubane structure and maintains the same set of cysteine ligands observed in more oxidized forms of the Fe protein. Specific Fe−Fe and S−S distances observed in the all-ferrous form and other forms of the Fe protein are presented in Table 2. The resolution of the all-ferrous Av2 structure (2.25 Å) is not sufficient to derive accurate $[4Fe\text{-}4S]^0$ cluster geometry parameters, such as the ones available for other oxidation states from model compounds (*28*). Although the differences are likely within the coordinate uncertainty, the all-ferrous Fe protein exhibits an overall distribution of four Fe−Fe distances greater than ∼2.65 Å and two distances less than ∼2.65 Å (Table 2). Since the geometry of the [4Fe-4S] cluster can be sensitive to the restraints used in the refinement of the cluster, the clusters in the all-ferrous and more oxidized form of Av2 were refined with the parameter set defined in Methods. Comparisons of the cluster geometry refined with the same protocol suggest that, relative to 1G5P, the all-ferrous Av2 has two large S−S distances (∼3.80 Å), an increased Fe1−Fe3 distance (2.79 Å), and a shorter Fe1−Fe4 distance (2.57 Å) (Table 2). For reference, the geometrical properties of [4Fe-4S]-type clusters, including average distances and

Table 3: Average Values for Geometrical Parameters for Protein-Bound [4Fe-4S] Clusters

interaction	average[a]	standard deviation[a]	no. of observations[a]	all-ferrous Av2[b]	1G5P[b]	1CP2[b]
Fe−S (Å)	2.29	0.05	492	2.33	2.31	2.30
Fe−SG (Å)	2.27	0.06	164	2.31	2.32	2.30
Fe−Fe (Å)	2.68	0.08	246	2.65	2.66	2.63
S−S (Å)	3.64	0.08	246	3.74	3.71	3.70
SG−SG (Å)	6.36	0.27	246	6.41	6.36	6.37
S−Fe−S (deg)	105.5	2.38	492	107.2	106.6	107.0
Fe−S−Fe (deg)	71.8	2.43	492	69.4	70.3	69.7
SG−Fe−S (deg)	113.0	6.22	492	111.6	111.3	111.8
CB−SG−Fe (deg)	108.8	6.78	164	109.0	107.4	110.5
Fe Td[c] volume (Å^3)	2.28	0.17	41	2.17	2.22	2.14
S Td volume (Å^3)	5.70	0.31	41	6.17	6.00	5.98
SG Td volume (Å^3)	29.91	1.40	41	30.82	28.69	30.29
[4Fe-4S] volume (Å^3)	9.27	0.47	41	9.23	9.29	9.06

[a] Average values from 41 [4Fe-4S] clusters in the PDB. The selection criteria for the proteins are described in the legend of Figure 2. [b] Average values for the indicated Fe protein structures. [c] Td = tetrahedral.

angles derived from 41 [4Fe-4S] cluster-containing proteins with four cysteine ligands, are shown in Table 3.

The all-ferrous Fe protein cluster has been studied previously by EXAFS, Mössbauer, and EPR techniques (*7*, *9*−*11*). The EXAFS curves of the Fe protein were best fit using two short (2.52 Å) Fe−Fe distances and one long (2.77 Å) Fe−Fe distance. A possible model with these distances is that of a compressed [4Fe-4S] cluster in which the vertical Fe−Fe distances are shorter and the horizontal Fe−Fe distances are longer (*9*). In the Mössbauer studies, one Fe site was found to be unique (*11*), although the correspondence between this site and the EXAFS-derived cluster model is not obvious. It is also not readily apparent how to unambiguously map the EXAFS- and Mössbauer-derived structural information onto the crystallographic structure, although the coordinate uncertainties in the diffraction analysis make this comparison difficult.

The presence of multiple forms of an iron−sulfur cluster in a crystal can lead to apparent structural distortions following refinement (*29*). These multiple forms are generally indicated by high *B*-factors and poor electron density for parts of the cluster. Since the all-ferrous Av2 cluster has a good uniform density with *B*-factors lower than its average main chain *B*-factors for the protein, this suggests the cluster exists predominantly in a single form.

Cluster Volumes. It has been reported (*9*) that the volume of the [4Fe-4S] cluster increases upon addition of electrons, although in general the structural consequences of changes in the oxidation state of a cluster will depend on the details of the bonding interactions (*30*). The Fe proteins have some of the smallest Fe tetrahedron volumes among [4Fe-4S] proteins, ranging from 2.15 to 2.20 Å^3 (Figure 2). In contrast, the sulfur tetrahedron in the all-ferrous Av2, due to the longer S−S bond lengths, has one of the largest volumes among [4Fe-4S] proteins (6.17 Å^3). An increase in the volume of the sulfur tetrahedron upon reduction from the $[4Fe\text{-}4S]^{2+}$ to $[4Fe\text{-}4S]^{+}$ state has also been observed in model compounds (*28*). The overall volume of the all-ferrous Av2 [4Fe-4S] cluster is, however, similar to those of other [4Fe-4S] protein clusters (Table 3).

To assess the sensitivity of these volumes to the refinement protocol, the [4Fe-4S] clusters of the all-ferrous Av2 and 1G5P were refined with three different restraints. For these refinements, all protein and solvent atoms were fixed, with the exception of the [4Fe-4S] cluster and the cysteine-containing loops (residues 96−98 and 131−133 in both monomers). Clusters in all-ferrous Av2 and 1G5P were refined using the following restraint schemes in the program CNS: (1) Fe−S distance restrained to 2.29 Å, with a penalty of 700 kcal mol^{-1} Å^{-2}, (2) Fe−S distance restrained to 2.33 Å, with a penalty of 700 kcal mol^{-1} Å^{-2}, and (3) no restraints. The Fe tetrahedron volumes were insensitive to the restraints that were employed, while the sulfur tetrahedron was found to fluctuate between 5.9 and 6.2 Å^3 in all-ferrous Av2 refinements and was found to have values ~0.2 Å^3 smaller in the 1G5P refinements. Although the sulfur

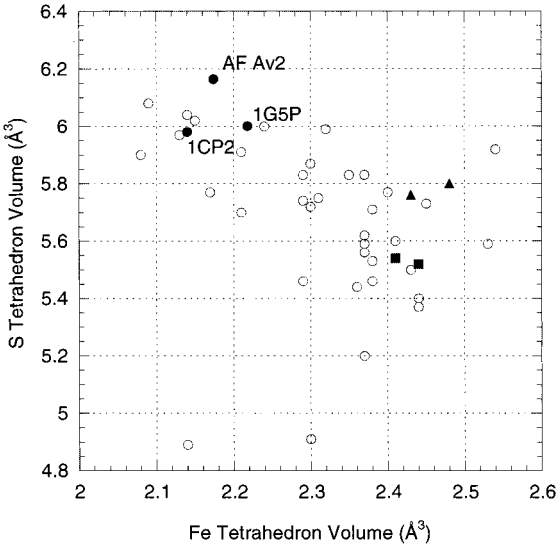

FIGURE 2: Variation in the volumes of the Fe and sulfur tetrahedron in [4Fe-4S] cluster-containing proteins of known structure. The all-ferrous Av2 has the largest sulfur tetrahedron volume, but one of the smallest Fe tetrahedron volumes. The overall all-ferrous Av2 cluster volume is comparable to those of other [4Fe-4S] clusters (Table 3). Only proteins with [4Fe-4S] clusters coordinated by four cysteine ligands and refined at resolutions of 2.5 Å or better were used in this analysis. The set contains the following PDB (*37*, *38*) files: all-ferrous (AF) Av2, 1G5P, 1CP2, 1BLU, 2FDN, 1FXR, 2FXB, 1VJW, 7FD1, 1ISU, 1HPI, 1CKU, 2NAP, 1AA6, 1QLA, 1AOP, 2ABK, 1DJN, 1MUY, 1AOR, 1B25, 1BOP, 1C4C, and 1H2R. Volumes for model compounds $[Fe_4S_4(SCH_2Ph)_4]^{2+/+}$ and $[Fe_4S_4(SPh)_4]^{2+/+}$ are also shown in the oxidized states (squares) and in the reduced states (triangles) (*28*). Tetrahedron volumes were calculated from the coordinates of the four defining atoms using eq 20 in section 2.2 of ref *39*.

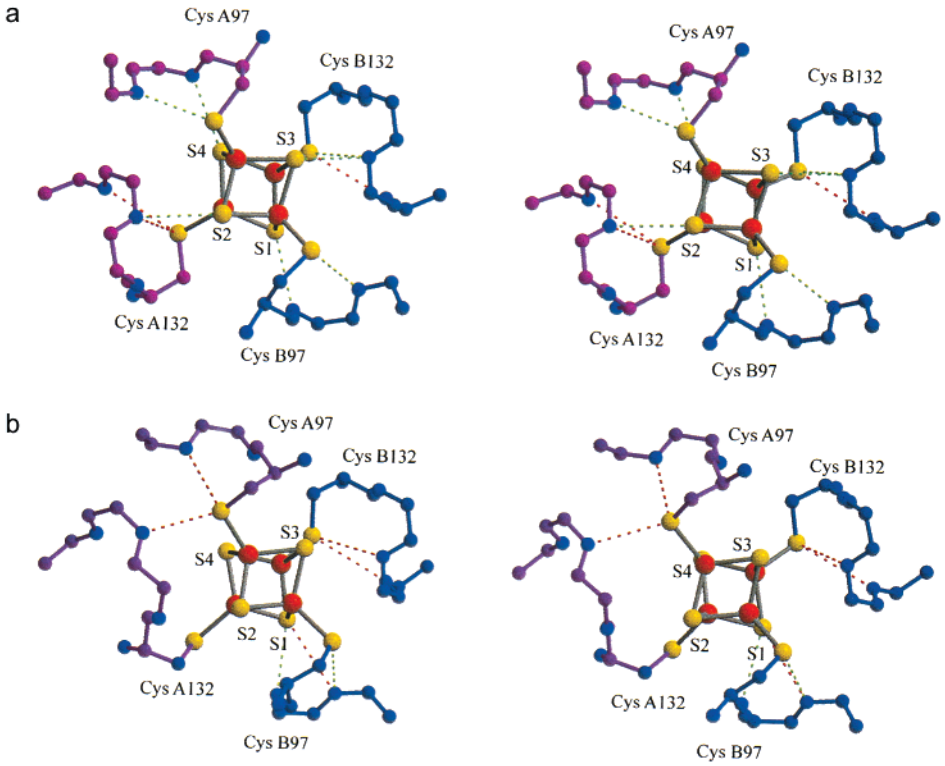

FIGURE 3: Stereodiagram of the [4Fe-4S] cluster environment in the (a) all-ferrous Av2 and (b) 1G5P structures. NH···S hydrogen bonds were defined when the N−S distance ≤ 3.5 Å and the N−H−S angle ≥ 120°. If the distance is between 3.5 and 3.7 Å or if the angle is less than 120°, then this interaction is termed an incipient bond. NH···S hydrogen bonds are in green, while the incipient hydrogen bonds are in red. Subunits A and B are in purple and blue, respectively, as in Figure 1. This figure was generated with Bobscript and Raster3D (*35*, *36*).

volumes appear to have an uncertainty of ∼0.2 Å^3 depending on the restraints, the sulfur volume of the all ferrous form of the cluster does appear consistently larger than the more oxidized 1G5P structure.

Accessible Surface. The [4Fe-4S] cluster in the Fe protein has the largest accessible surface area among [4Fe-4S] cluster-containing proteins of known structure. While most known [4Fe-4S] clusters are completely buried within proteins, the accessible cluster surface areas in the Fe protein structures are 13.5, 14.0, and 18.2 Å^2 for the all-ferrous Av2, 1G5P, and 1CP2 structures, respectively. For these calculations, the accessible surface areas of the clusters were calculated with program SURFACE (*18*) using radii of 0.65 and 1.8 Å for the Fe and S atoms, respectively. Although there is no evidence that surface accessibility correlates with the ability of the [4Fe-4S] cluster to adopt the +2, +1, and 0 oxidation states, solvent exposure has been reported to facilitate reduction of the Fe center in rubredoxin (*31*).

NH···S Hydrogen Bonds. NH···S hydrogen bonds between main chain amide groups and sulfur atoms of the cluster and thiol groups of cysteine ligands (*32*) are present in all Fe protein structures. For this analysis, NH···S hydrogen bonds were defined as having an N−S distance of ≤3.5 Å and an N−H−S angle of ≥120°. Incipient hydrogen bonds were defined as having an N−S distance between 3.5 and 3.7 Å or having an N−H−S angle between 100° and 120°. The all-ferrous Av2 structure has seven real and three incipient hydrogen bonds (Figure 3A); while the 1G5P structure has only three real and four incipient hydrogen bonds (Figure 3B), the 1CP2 structure has five real and six incipient hydrogen bonds and the 1N2C structure has four real and two

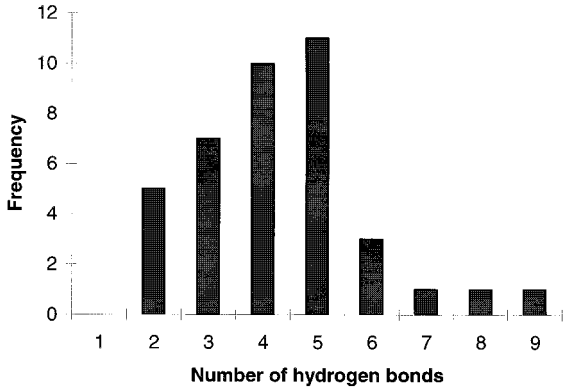

FIGURE 4: Histogram of the number of NH···S hydrogen bonds to the cluster observed in structures of [4Fe-4S] cluster-containing proteins. Only the hydrogen bonds defined as "real" are shown. The set of proteins used is defined in the legend of Figure 2, and the NH···S hydrogen bonds are identified as described in the legend of Figure 3.

incipient hydrogen bonds. The average number of NH···S hydrogen bonds derived from other known [4Fe-4S] cluster-containing proteins is four real and three incipient hydrogen bonds (Figure 4). NH···S hydrogen bonds could help stabilize the more reduced form of the redox centers, as recently described in detail for the Fe(CysS)$_4$ center in rubredoxin (*33*). While the larger number of NH···S interactions in the all-ferrous Av2 could help stabilize the reduced [4Fe-4S]^0 state of the cluster, a similar number of NH···S hydrogen bonds have also been observed in other [4Fe-4S] cluster-containing structures (PDB entries 1DJN, 1VJW, and 2FDN).

CONCLUSIONS

The [4Fe-4S] cluster in the all-ferrous Av2 does not experience any changes in coordination upon reduction to the $[4Fe\text{-}4S]^0$ oxidation state, unlike the P cluster of the nitrogenase MoFe protein (*34*). While Mössbauer spectroscopy suggests one unique Fe site is present in the all-ferrous cluster, such a site could not be identified in the crystal structure. The distortion of the all-ferrous [4Fe-4S] cluster cannot be easily classified; two S−S distances become slightly longer, but the overall volume of the cluster remains nearly constant. The number of NH···S hydrogen bonds to the cluster and thiol groups of cysteine ligands is higher in the all-ferrous Av2 than in most other [4Fe-4S] proteins. There are, however, a few proteins with similar numbers of cluster hydrogen bonds. One (so far) unique property of the Fe protein cluster is its solvent accessibility. The Fe protein has the most surface accessible cluster of all known [4Fe-4S] proteins, suggesting that the solvent accessibility of the all-ferrous Av2 cluster might play a role in its ability to exist in all three oxidation states. Aside from these correlations, perhaps the most striking aspect of this structural analysis is how closely the all-ferrous Fe protein resembles more oxidized forms. Remarkably, the Fe protein can accommodate three oxidation states of the [4Fe-4S] cluster with only minimal changes in protein or cluster conformation.

ACKNOWLEDGMENT

We thank Tina M. Iverson for assistance with data collection and James B. Howard for discussions.

REFERENCES

1. Howard, J. B., and Rees, D. C. (1994) *Annu. Rev. Biochem. 63*, 235−264.
2. Burgess, B. K., and Lowe, D. J. (1996) *Chem. Rev. 96*, 2983−3011.
3. Seefeldt, L. C., and Dean, D. R. (1997) *Acc. Chem. Res. 30*, 260−266.
4. Smith, B. E. (1999) *Adv. Inorg. Chem. 47*, 159−218.
5. Rees, D. C., and Howard, J. B. (2000) *Curr. Opin. Chem. Biol. 4*, 559−566.
6. Watt, G. D., and Reddy, K. R. N. (1994) *J. Inorg. Biochem. 53*, 281−294.
7. Angove, H. C., Yoo, S. J., Burgess, B. K., and Münck, E. (1997) *J. Am. Chem. Soc. 119*, 8730−8731.
8. Angove, H. C., Yoo, S. J., Münck, E., and Burgess, B. K. (1998) *J. Biol. Chem. 273*, 26330−26337.
9. Musgrave, K. B., Angove, H. C., Burgess, B. K., Hedman, B., and Hodgson, K. O. (1998) *J. Am. Chem. Soc. 120*, 5325−5326.
10. Yoo, S. J., Angove, H. C., Burgess, B. K., Münck, E., and Peterson, J. (1998) *J. Am. Chem. Soc. 120*, 9704−9705.
11. Yoo, S. J., Angove, H. C., Burgess, B. K., Hendrich, M. P., and Münck, E. (1999) *J. Am. Chem. Soc. 121*, 2534−2545.
12. Erickson, J. A., Nyborg, A. C., Johnson, J. L., Truscott, S. M., Gunn, A., Nordmeyer, F. R., and Watt, G. D. (1999) *Biochemistry 38*, 14279−14285.
13. Holm, R., Kennepohl, P., and Solomon, E. (1996) *Chem. Rev. 96*, 2239−2314.
14. Burgess, B. K., Jacobs, D. B., and Stiefel, E. I. (1980) *Biochim. Biophys. Acta 614*, 196−209.
15. Seefeldt, L. C., and Ensign, S. A. (1994) *Anal. Biochim. 221*, 379−386.
16. Georgiadis, M. M., Komiya, H., Chakrabarti, P., Woo, D., Kornuc, J. J., and Rees, D. C. (1992) *Science 257*, 1653−1659.
17. Navaza, J. (1994) *Acta Crystallogr. A50*, 157−163.
18. Bailey, S. (1994) *Acta Crystallogr. D50*, 760−763.
19. de LaFortelle, E., and Bricogne, G. (1997) *Methods Enzymol. 276*, 472−494.
20. Cowtan, K. (1994) *Joint CCP4 and ESF-EACBM Newsletter on Protein Crystallography 31*, 34−38.
21. Jones, T. A., Zou, J. Y., Cowan, S. W., and Kjeldgaard, M. (1991) *Acta Crystallogr. A47*, 110−119.
22. Brunger, A. T. (1992) *X-PLOR Manual Version 3.1: A System for X-ray Crystallography and NMR*, Yale University Press, New Haven, CT.
23. Laskowski, R. A., MacArthur, M. W., Moss, D. S., and Thornton, J. M. (1993) *J. Appl. Crystallogr. 26*, 283−291.
24. Schlessman, J. L., Woo, D., Joshua-Tor, L., Howard, J. B., and Rees, D. C. (1998) *J. Mol. Biol. 280*, 669−685.
25. Schindelin, H., Kisker, C., Schlessman, J. L., Howard, J. B., and Rees, D. C. (1997) *Nature 387*, 370−376.
26. McKenna, C. E., Gutheil, W. G., and Wei, S. (1991) *Biochim. Biophys. Acta 1075*, 109−117.
27. Nave, C. (1995) *Rad. Phys. Chem. 45*, 483−490.
28. Berg, J. M., and Holm, R. H. (1982) in *Iron−Sulfur Proteins* (Spiro, T. G., Ed.) pp 1−66, John Wiley, New York.
29. Sridhar, V., Prasad, S. G., Burgess, B. K., and Stout, C. D. (1998) *J. Biol. Inorg. Chem. 3*, 140−149.
30. Han, J., Beck, K., Ockwig, N., and Coucouvanis, D. (1999) *J. Am. Chem. Soc. 121*, 10448−10449.
31. Xiao, Z., Maher, M. J., Cross, M., Bond, C. S., Guss, M. J., and Wedd, A. G. (2000) *J. Biol. Inorg. Chem. 5*, 75−84.
32. Adman, E. T., Watenpaugh, K. D., and Jensen, L. H. (1975) *Proc. Natl. Acad. Sci. U.S.A. 72*, 4854−4858.
33. Eidsness, M. K., Burden, A. E., Richie, K. A., Kurtz, D. M., Jr., Scott, R. A., Smith, E. T., Ichiye, T., Beard, B., Min, T., and Kang, C. (1999) *Biochemistry 38*, 14803−14809.
34. Peters, J. W., Stowell, M. H., Soltis, S. M., Finnegan, M. G., Johnson, M. K., and Rees, D. C. (1997) *Biochemistry 36*, 1181−1187.
35. Esnouf, R. M. (1997) *J. Mol. Graphics 15*, 133−138.
36. Merritt, E. A., and Bacon, D. J. (1997) *Methods Enzymol. 277*, 505−524.
37. Sussman, J. L., Lin, D., Jiang, J., Manning, N. O., Prilusky, J., Ritter, O., and Abola, E. E. (1998) *Acta Crystallogr. D54*, 1078−1084.
38. Berman, H. M., Westbrook, J., Feng, Z., Gilliland, G., Bhat, T. N., Weissig, H., Shindyalov, I. N., and Bourne, P. E. (2000) *Nucleic Acids Res. 28*, 235−242.
39. Kaspar, J. S., and Lonsdale, K. (1972) *International Tables for X-ray Crystallography*, 3rd ed., Vol. II, D. Reidel, Dordrecht, The Netherlands.

BI0016467